Nonlinearity-Compensation Extended Kalman Filter for Handling Unexpected Measurement Uncertainty in Process Tomography

Jeong-Hoon Kim*, Umer Zeeshan Ijaz*, Bong-Seok Kim*, Min-Chan Kim**, Sin Kim*** and Kyung-Youn Kim*

* Department of Electrical & Electronic Engineering
** Department of Chemical Engineering
*** Department of Nuclear and Energy Engineering
Cheju National University, Jeju 690-756, Korea
(Tel: +82-64-754-3664; E-mail: kyungyk@cheju.ac.kr)

Abstract: The objective of this paper is to estimate the concentration distribution in flow field inside the pipeline based on electrical impedance tomography. Special emphasis is given to the development of dynamic imaging technique for two-phase field undergoing a rapid transient change. Nonlinearity-compensation extended Kalman filter is employed to cope with unexpected measurement uncertainty. The nonlinearity-compensation extended Kalman filter compensates for the influence of measurement uncertainty and solves the instability of extended Kalman filter. Extensive computer simulations are carried out to show that nonlinearity-compensation extended Kalman filter has enhanced estimation performance especially in the unexpected measurement environment.

Keywords : Nonlinearity-Compensation Extended Kalman Filter, Extended Kalman Filter, Electrical Impedance Tomography, Dynamic Image Reconstruction, Process Tomography, Root Mean Square Error.

1. INTRODUCTION

Process tomography (PT) involves using tomographic imaging methods to manipulate measurement data from sensors in order to obtain precise quantitative information on the inaccessible regions. The region may be for example, a furnace, a mixing chamber or a pipeline, and the tomography imaging can be based on electromagnetic or acoustic sounding or radioscopic imaging. *In essence, the goal is to estimate computationally the multidimensional distribution of some physical parameter based on indirect observations from the boundary of the object* [10].

Typical features of industrial processes are a high noise level and rapid changes in the object. Thus, the imaging modality has to be sufficiently fast and robust for proper dynamical change of the target.

We consider the problem of imaging the concentration distribution of a given substance in a fluid moving in a pipeline based on static or low frequency measurements on the surface of the pipe. Set of contact electrodes are attached to the surface of the pipe, and are electronically insulated from the pipe. Electric currents are injected through these electrodes and the corresponding voltages needed to maintain the currents are recorded. Hence the imaging modality used in this case is Electrical Impedance Tomography (EIT).

As compared to the traditional EIT, in the present case, the object is very rapidly changing during the data acquisition; hence a reasonable spatiotemporal resolution is desirable. Rather than considering the inverse problem as a traditional tomography reconstruction problem, we view the problem as *state estimation problem*. The concentration distribution is considered as a stochastic process, or a state of the system, that satisfies a stochastic differential equation. This equation is referred to as *state evolution equation*. We model the concentration distribution by the convection-diffusion equation, which allows an approximation of the velocity field.

We consider here approximating a fast flow with a laminar flow and compute the velocity field by solving the Navier-Stokes equations numerically. Conventionally, the state estimation is performed by using Kalman filter, fixed-lag Kalman smoother or extended Kalman filter (EKF) algorithm. In our case we have used nonlinear-compensation extended Kalman filter (NLCEKF). The work flow is explained in Fig .1.

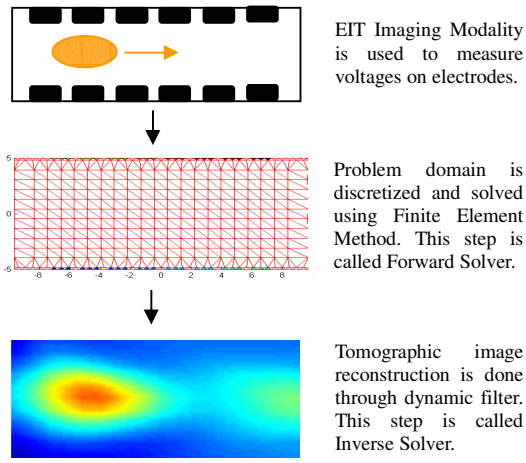

Fig. 1. Workflow of the typical reconstruction process in Process Tomography (In this case, a straight pipe is considered).

The purpose of the present work is to apply NLCEKF to dynamic PT for performance enhancement of the dynamic image reconstruction in the presence of unexpected measurement uncertainty. This unexpected measurement

uncertainty can be any external short-living perturbation in the measurement data. Usually such perturbations cause the conventional EKF to diverge and estimation performance is deteriorated drastically. The instability of EKF in such cases is a major bottle neck for such perturbed systems. In order to tackle this problem, NLCEKF is employed in Inverse Solver which has already proved its might compared to EKF in optimization problems related to other walks of life, especially Target Motion Analysis. See [11].

The rest of the paper is organized as follows. In section 2, we have explained the discrete state-space dynamic model considering convection-diffusion model. For the brevity of discussion, we have kept our discussion short. Further details on PT can be found in [6-11]. Section 3 deals with EIT applied to PT. Only the Observation model is discussed. Section 4 deals with ins and outs of NLCEKF. Section 5 deals with the simulation and comparison of results.

2. DISCRETE STATE-SPACE DYNAMIC MODEL

In the case of moving fluids into the straight pipe the concentration distribution $c = c(x,t)$ can be modeled by the stochastic convection-diffusion equation as follows

$$\frac{\partial c}{\partial t} = \kappa\Delta c - \vec{v}\cdot\nabla c + \mu \tag{1}$$

where $\kappa = \kappa(x)$ is the diffusion coefficient, $\vec{v} = \vec{v}(x)$ is the velocity of the flow and $\mu = \mu(x,t)$ is the modeling errors.

Incompressibility is defined as

$$\nabla\cdot\vec{v} = 0 \tag{2}$$

Which represents that density of fluid is same throughout the field and it does not change with time.

Boundary condition is defined as

$$\frac{\partial c}{\partial n} = 0 \qquad \text{at } x \in \left(\partial\Omega \setminus \partial\Omega_{in\cup wall}\right) \tag{3}$$

which means that there is no diffusion through the pipe walls and the input boundary, so that the outward unit normal is orthogonal to the velocity of the flow in the wall.

Initial conditions are

$$c(x,0) = c_0(x) \tag{4}$$

$$c(x,t) = c_{in}(t) \qquad \text{at } x \in \partial\Omega_{in} \tag{5}$$

(4) represents the initial value at $t = 0$ and (5) represents the Dirichlet condition which can be taken into account by using the Petrov-Galerkin method.

(1) can be solved in discrete form using the Petrov-Galerkin method and the backward (implicit) Euler method as

$$c_{t+1} = \overline{F}c_t + \overline{s}_{t+1} + \overline{w}_{t+1} \tag{6}$$

where $\overline{F} \in \Re^{N\times N}$ is the state transition matrix, $\overline{s}_{t+1} \in \Re^{N\times 1}$ is the input vector and $\overline{w}_{t+1} \in \Re^{N\times 1}$ is the disturbance vector.

Here, we assume a linear model satisfying

$$\sigma(x,t) = \lambda c(x,t) \tag{7}$$

The reason for this assumption of concentration $c(x,t)$ is to estimate it by electrical impedance tomography. Since there is a direct linear relationship between conductivity and concentration, hence by using EIT, we can reconstruct conductivity and then can map concentration against it. *This is the main reason why EIT is used as imaging modality.*

We can obtain the discrete state-space model as follows

$$\sigma_{t+1} = \overline{F}^*\sigma_t + \overline{s}^*_{t+1} + \overline{w}^*_{t+1} \tag{8}$$

where $\overline{F}^* \in \Re^{N\times N}$, $\overline{s}^*_{\tilde{t}+1} \in \Re^{N\times 1}$ and $\overline{w}^*_{\tilde{t}+1} \in \Re^{N\times 1}$ are functions to relate between the resistivity $\sigma(x,t)$ and $c(x,t)$ linearly.

Now, let us consider the case in which the time step is too large in comparison to the velocity of fluid, for that case, the backward Euler method is inaccurate while solving the convection-diffusion equation numerically by the evolution model.

Assume the time step $\Delta t/n$ is small enough to obtain a feasible numerical solution for the stochastic convection-diffusion equation. Here, the state equation corresponding to the time step $\Delta t/n$ is used as follows. [8]

$$\sigma_{\tilde{t}+1} = F\sigma_{\tilde{t}} + s_{\tilde{t}+1} + w_{\tilde{t}+1} \tag{9}$$

Where Δt is the time step used in the evolution model.

We can obtain the next step as

$$\begin{aligned}\sigma_{\tilde{t}+2} &= F\sigma_{\tilde{t}+1} + s_{\tilde{t}+1} + w_{\tilde{t}+1}\\ &= F\left(F\sigma_{\tilde{t}} + s_{\tilde{t}+1} + w_{\tilde{t}+1}\right) + s_{\tilde{t}+2} + w_{\tilde{t}+2}\\ &= F^2\sigma_{\tilde{t}} + \left(Fs_{\tilde{t}+1} + s_{\tilde{t}+2}\right) + \left(Fw_{\tilde{t}+1} + w_{\tilde{t}+2}\right)\end{aligned} \tag{10}$$

Similarly,

$$\begin{aligned}\sigma_{\tilde{t}+3} &= F^3\sigma_{\tilde{t}} + \left(F^2 s_{\tilde{t}+1} + Fs_{\tilde{t}+2} + s_{\tilde{t}+3}\right)\\ &\quad + \left(F^2 w_{\tilde{t}+1} + Fw_{\tilde{t}+2} + w_{\tilde{t}+3}\right)\end{aligned} \tag{11}$$

Furthermore,

$$\begin{aligned}\sigma_{\tilde{t}+n} &= F^n\sigma_{\tilde{t}} + \left(F^{n-1} + \cdots + F^0\right)s_{\tilde{t}+n}\\ &\quad + \left(F^{n-1} + \cdots + F^0\right)w_{\tilde{t}+n}\\ &= F^n\sigma_{\tilde{t}} + \Gamma_{\tilde{t}+n}\left(s_{\tilde{t}+n} + w_{\tilde{t}+n}\right)\end{aligned} \tag{12}$$

where $\Gamma_{\tilde{t}+n} \in \Re^{N\times N}$ is $\left(F^{n-1} + \cdots + F^0\right)$.

Hence, we can obtain the *state evolution equation* as

$$\sigma_{t+1} = F^n \sigma_t + \Gamma_{t+1}(s_{t+1} + w_{t+1}) \quad (13)$$

Where $F^n \in \Re^{N\times N}$ is the evolution matrix, $s_{t+1} \in \Re^{N\times 1}$ is the input vector and $w_{t+1} \in \Re^{N\times 1}$ is the disturbance vector.

3. ELECTRICAL IMPEDANCE TOMOGRAPHY

When electrical currents $I_l (l = 1,2,...,L)$ are injected into the object $\Omega \in R^2$ through the electrodes $e_l (l = 1,2,...,L)$ attached on the boundary $\partial\Omega$ with the internal structure, the conductivity distribution $\sigma(x, y)$ is known for Ω, then corresponding electrical potential $u(x, y)$ on the Ω can be determined uniquely from the partial differential equation, which can be derived from the Maxwell equations as

$$\nabla \cdot (\sigma \nabla u) = 0 \qquad \text{in } \Omega \quad (14)$$

with the following boundary conditions based on the complete electrode model:

$$u + z_l \sigma \frac{\partial u}{\partial n} = U^{(l)} \quad \text{on } e_l, \quad l = 1,2,...,L \quad (15)$$

$$\int_{e_l} \sigma \frac{\partial u}{\partial n} dS = I^{(l)}, \quad l = 1,2,...,L \quad (16)$$

$$\sigma \frac{\partial u}{\partial n} = 0 \qquad \text{on } \partial\Omega \setminus \bigcup_{l=1}^{L} e_l \quad (17)$$

where, z_l is the effective contact impedance between lth electrode and electrolyte, $U^{(l)} = U^{(l)}(t_k)$ is the potential on the lth electrode at time k, $I^{(l)} = I^{(l)}(t_k)$ is the injected current on the lth electrode at time k, e_l is lth electrode, n is outward unit normal, and L is the total number of electrodes.

Furthermore, the following two constraints for the injected currents and measured voltages are needed to ensure the existence and uniqueness of the solution:

$$\sum_{l=1}^{L} I^{(l)} = 0 \quad (18)$$

$$\sum_{l=1}^{L} U^{(l)} = 0 \quad (19)$$

The computation of the potential $u(x, y)$ on the Ω and the voltages $U^{(l)}$ on the electrodes for the given conductivity distribution $\sigma(x, y)$ and boundary conditions is called the forward problem. In general, the forward problem cannot be solved analytically, thus we have to resort to the numerical method. There are different numerical methods such as the finite difference method (FDM), boundary element method (BEM), and finite element method (FEM). In this paper, we used the FEM to obtain numerical solution. In FEM, the object area is discretized into sufficiently small elements having a node at each corner and it is assumed that the conductivity distribution is constant within each element. The potential U_k at each node and the electrodes at time k, defined by the vector

$$U_k = R(\sigma_k) I_k \quad (20)$$

where, $R(\sigma_k)$ and I_k are the functions of the conductivity distribution into the object and the injected currents through the electrodes at time k, respectively. For more details on the forward solution and the FEM approach, see [8,10]

Here, let $U_k \in R^{L\times 1}$, defined as

$$U_k \equiv \left[U_k^1 U_k^2 ... U_k^L\right]^T \quad (21)$$

be the measurement voltages on the surface and internal electrodes induced by the k^{th} current pattern. Then the *observation equation* can be described as the following nonlinear mapping with measurement noise

$$U_k = V_k(\sigma_k) + v_k \quad (22)$$

where the measurement noise v_k is also assumed to be white Gaussian noise with covariance.

For details on FEM forward solver for EIT, consult chapter 3 in [12].

4. INVERSE SOLVER BASED ON NONLINEARITY-COMPENSATION EXTENDED KALMAN FILTER

4.1 NonLinear-Compensation Extended Kalman Filter algorithm

From (13) and (22), we can obtain the dynamic equations as followings

$$\sigma_k = F^n \sigma_{k-1} + \Gamma_k (s_k + w_k) \quad (23)$$

$$U_k = V_k(\sigma_k) + v_k \quad (24)$$

In EKF the state estimation is optimized as minimizing the cost functional as follows

$$\begin{aligned} J(\sigma_k) &= \frac{1}{2} E\{\varepsilon_{\sigma_k}^T \varepsilon_{\sigma_k}\} \\ &= \frac{1}{2}\{(z_k - h_k(\sigma_k))^T R_k^{-1} (z_k - h_k(\sigma_k)) \\ &\quad + (\sigma_k - \sigma_{k|k-1})^T P_{k|k-1}^{-1} (\sigma_k - \sigma_{k|k-1})\} \end{aligned} \quad (25)$$

where $E\{\cdot\}$ is the expectation, $\sigma_{k|k-1}$ is the latest predicted state and $R_k \in \Re^{L\times L}$ is $E\{n_k n_k^T\}$, so that the measurement noise covariance. $P_{k|k-1} \in \Re^{N\times N}$ is the time-updated error covariance matrix, which is defined by

$$P_{k|k-1} \equiv E\{(\sigma_k - \sigma_{k|k-1})(\sigma_k - \sigma_{k|k-1})^T\} \quad (26)$$

Linearizing (8) about the current predicted state $\sigma_{k|k-1}$ we obtain

$$U_k = V_k(\sigma_{k|k-1}) + H_{\sigma_{k|k-1}}(\sigma_k - \sigma_{k|k-1}) + H.O.Ts + v_k \quad (27)$$

where $H.O.Ts$ represent the higher-order terms which will be considered as additional noise, $H_{\sigma_{k|k-1}} \in \Re^{L\times N}$ is the Jacobian matrix defined by

$$H_{\sigma_{k|k-1}} \equiv \left.\frac{\partial V_k}{\partial \rho}\right|_{\rho=\rho_{k|k-1}} \quad (28)$$

where ρ is the resistivity i.e, $1/\sigma$.
Now we define the pseudo-measurement as

$$y_k \equiv U_k - V_k(\sigma_{k|k-1}) + H_{\sigma_{k|k-1}}\sigma_{k|k-1} \quad (29)$$

And hence, we can develop the linearized observation equation as following

$$y_k = H_{\sigma_{k|k-1}}\sigma_k + v_k \quad (30)$$

In comparison to the cost functional defined for image reconstruction for EKF, *the cost functional for NLCEKF* is computed as follows

$$J(\hat{\sigma}_{k|k}) = \frac{1}{2}\{(z_k - H_k\hat{x}_{k|k})^T R_k^{-1}(z_k - H_k\hat{x}_{k|k}) + (\hat{\sigma}_{k|k} - \hat{\sigma}_{k|k-1})^T P_{k|k-1}^{-1}(\hat{\sigma}_{k|k} - \hat{\sigma}_{k|k-1})\} \quad (31)$$

By minimizing the cost functional and solving for the updates of the associated covariance matrices, we obtain the NLCKEF algorithm which consists of the following two steps similar to EKF.

(i) Measurement Update Step (Filtering)

$$K_k = P_{k|k-1}H_i^T\left[H_k P_{k|k-1}H_k^T + R_k\right]^{-1} \quad (32)$$

$$\sigma_{k|k} = \sigma_{k|k-1} + \alpha K_k\left(y_k - H_k\sigma_{k|k-1}\right) \quad (33)$$

$$C_{k|k} = (I - \beta^2 K_k H_k)P_{k|k-1} \quad (34)$$

(ii) Time Update Step (Prediction)

$$P_{k+1|k} = F_k P_{k|k} F_k^T + \Gamma_k Q_k \Gamma_k^T \quad (35)$$

$$\sigma_{k+1|k} = F_k\sigma_{k|k} + s_k \quad (36)$$

where $F_k = F_k^n \in \Re^{N\times N}$ is the evolution matrix and $s_k \in \Re^{N\times 1}$ is the input vector. α is used to adjust the Kalman gain K_k in equation (33), the range of α is $0 \sim 2$ and β is determined by

$$\beta = \begin{cases} \alpha & : \ 0 \le \alpha \le 1 \\ 2-\alpha & : \ 1 < \alpha \le 2 \end{cases} \quad (37)$$

Here, the coefficient α adjusts an optimization value of the Kalman gain according to the uncertainty of a measurement value.
When $\alpha = 1$, the results obtained from state estimation problem are equal to the result of conventional EKF. This means that NLCEKF is working like conventional EKF.
When $\alpha = 0$, the state is not updated. So, a predicted state is used instead of a filtered state. This means that when the system is estimated by the uncertain measurement noise the predicted state is not updated.
Since β is a parameter adjusting the error covariance matrix of equation (34) depending on α so the more α is far from 1 the more β is decreased.
Also, the process error covariance $Q_k \in \Re^{N\times N}$ and the measurement error R_k is determined by

$$Q_k = E\{w_k w_k^T\} \quad (38)$$

$$R_k = E\{v_k v_k^T\} \quad (39)$$

Where w_k is the White Gaussian Noise for the process at k time step and v_k is the White Gaussian Noise for measurement data at k time step.

4.2 Temporal Regularization

Because the dynamic reconstruction is dependent on time, so for reconstruction we just need temporal regularization, not spatial regularization.
Temporal regularization is considered in three components as follows

$$Q_{\mu_k} = \beta_\mu I \quad (40)$$

$$Q_{\eta_k} = \beta_\eta I \quad (41)$$

$$Q_{\eta_k'} = \beta_{\eta'} I \quad (42)$$

(40) is the stochastic nature of the diffusion, we assume the noise μ_k is uncorrelated and having constant variance in all

parts of the phantom. (41) represents an uncertain oscillatory component in the pipe inlet and (42) means the input stream is assumed to be very slowly varying in the time scale.
Hence, process error covariance is represented as follows

$$Q_k = YQ_{\mu_k}Y^T + DQ_{\eta_k}D^T + HQ_{\eta_k'}H^T \qquad (43)$$

where the matrices Y,D and H are the finite element matrices mapping the random vectors μ_k, η_k and η_k', respectively. [8,10] Here, β_μ, β_η and $\beta_{\eta'}$ is obtained empirically.

5. SIMULATION RESULTS

We have carried out the computer simulations on synthetic data to evaluate the reconstruction performance of NLCEKF. The computer simulation was carried out on a straight pipe including varying measurement noise. Parabolic velocity field are also considered.

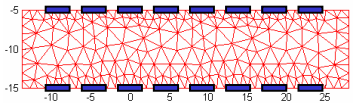

Fig.2. Straight pipe-type FEM mesh(Mesh for inverse problem) and electrodes.

The FEM meshes used for the inverse solvers are shown in Fig. 2. We have used the straight pipe-type model with a mesh size of 394 elements and 250 nodes. We have used a fine mesh near the boundaries in order to make a good sensitivity analysis considering the complications involved in measurement. Electrodes are located on each side of pipe as a set of 8, the total numbers being 16.

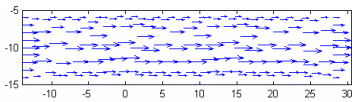

Fig. 3. Computed velocity field inside straight pipe.

The velocity field is assumed to satisfy the conditions of parabolic flow as shown in Fig 3. Here, the equation with respect to the flow across x-direction is developed as follows

$$v_x(x,y) = v_{x,mean} \cdot \left[1 - \left(\frac{y - y_0}{R}\right)^2\right] \qquad (44)$$

Where $v_{x,mean}$ is the spatial average velocity in x-direction. y_0 is the index of y as distance from center of the pipe and R is the inner radius of the pipe.
It is also assumed that the initial average velocity in x-direction, $v_{x,mean}$ is $450\ cms^{-1}$. The initial setting for parameters used in the simulation is as following. The contact impedance z used in the simulation is $0.001\ \Omega$. The convection coefficient χ is 5×10^1. Number of frames for current injection is 5. The minimum value of conductivity distribution is set to $1/200\ \ \Omega^{-1}cm^{-1}$ and the maximum value of conductivity distribution is set to $1/400\ \ \Omega^{-1}cm^{-1}$. The injection pattern uses the "opposite" method. The time to measure voltages of a pattern is set to $5\ ms$.
Next, simulations were carried out to analyze effects on the image reconstruction by the uncertain measurement noise on the following data.
Initial assumed conductivity is $\sigma_0 = 0.0043\ \ \Omega^{-1}cm^{-1}$, initial assumed covariance for the initial state vector is $C_{0|0} = (0.1 * \sigma_0)^2 I$, the average velocity in x-direction is assumed constant for given time. The covariances with respect to the temporal regularization are $\beta_\mu = 5\times10^{-3}$ and $\beta_\eta = 2\times10^{-6}$, $\beta_{\eta'} = 0$. The measurement noise v_k is set to 0.1% of the difference between the maximum and the minimum value of the voltage without the noise. The unexpected measurement uncertainty noise consisted of White-Gaussian Noise that occurs for 5 time steps from 30th step onward.

For the sake of comparison of performance of the reconstruction algorithm, root mean square error (RMSE) is defined as following

$$RMSE(V(\sigma_k)) = \sqrt{\frac{(U_{true} - V(\sigma_k))^T \cdot (U_{true} - V(\sigma_k))}{(U_{true})^T \cdot (U_{true})}} \qquad (45)$$

We have considered two cases: 3% and 10% of unexpected measurement uncertainty noise of the difference between the maximum and the minimum value of the voltage without the noise.

5.1 Simulation Results : Analysis of unexpected measurement uncertainty

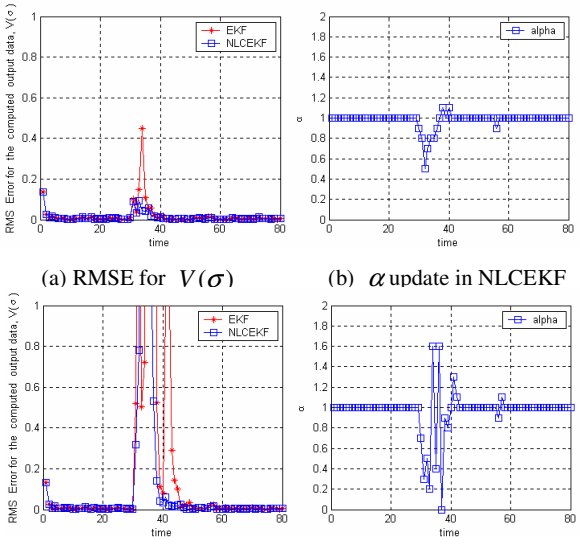

(a) RMSE for $V(\sigma)$ (b) α update in NLCEKF

(c) RMSE for $V(\sigma)$ (d) α update in NLCEKF

Fig. 4. (a) and (c) represent RMSE for $V(\sigma)$ with the uncertain measurement noise 3% and10% respectively. (b) and (d) represent the variation in α cases for the two cases

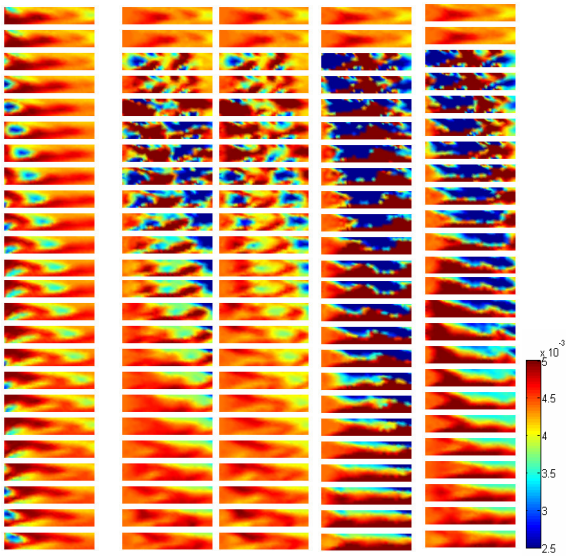

(a)True (b)EKF (c)NLCEKF (d)EKF (e)NLCEKF

Fig. 5. Image reconstructed according to each uncertain measrement noise (between the interval of 28th and 51th time steps). (a) True Image Frame. (b) and (c) Image reconstructed with 3% uncertain measurement noise. (d) and (e) Image reconstructed with 10% uncertain measurement noise.

In Fig. 4 and Fig. 5, we can see that when unexpected measurement uncertainty occurs, there is a little fluctuation in RMSE with NLCEKF as compared to EKF since EKF algorithm just selects the Kalman gain that optimizes linearly and can not optimize against the nonlinearity phenomenon. On the contrary, NLCEKF modifies the Kalman gain by α, and estimation quality is better than EKF in case of nonlinearity.

6. CONCLUSIONS

A dynamic impedance imaging technique is applied to the visualization of two-phase flow field undergoing rapid transient. In this paper, nonlinear-compensation extended Kalman filter is employed to cope with the unexpected measurement uncertainty. We have pointed out the enhancements in the estimation for the cases when uncertain noise exists in the system. In those cases, nonlinear-compensation extended Kalman filter is far more effective than conventional extended Kalman filter in terms of spatial resolution of reconstructed image. For the verification of our hypothesis, we have simulated a bubbly flow and a slug flow and reconstructed the pipe-type images with synthesized data and have compared the result based on root mean square error. The reconstructed images indicate a good possibility of dynamic process tomography system with integrated nonlinear-compensation extended Kalman filter to the visualization of rapid transient two-phase system undergoing sudden perturbation.

7. ACKNOWLEDGMENTS

The work was supported by grant No. R01-2004-000-0040-0 (2004) from the Basic Research Program of the Korea Science & Engineering Foundation.

8. REFERENCES

[1] Arthur Gelb, “Applied Optimal Estimation”, MIT Press, Cambridge,1974.

[2] 이윤준, 김경연, 김신, 김민찬, 김호찬, 박재우, 이정훈, 이헌주, 천원기, 최민주, “이상유동장 가시화를 위한 ET(Electrical Tomography) 기법 개발에 관한 연구”, 과학기술부 최종보고서, Jul. 2001.

[3] 김봉석, “확장 칼만 필터를 이용한 전기 임피던스 단층촬영법” , 제주대학교 전기전자공학과 석사학위논문, Dec. 2000.

[4] 강숙인, “Dynamic Electrical Impedance Tomography with Prior Information”, 제주대학교 전기전자공학과 석사학위논문, Dec. 2002.

[5] R.A.Williams, M.S.Beck, “Process Tomography : Principles, techniques and applications”, Butterworth-Heinemann Ltd, 1995.

[6] A. Seppänen, M. Vauhkonen, J.P. Kaipio, E. Somersalo, "Inference of velocity fields based on tomographic measurements in process industry", *4th International Conference on Inverse Problems in Engineering*, Rio de Janeiro, Brazil, 2002.

[7] A. Seppänen, M. Vauhkonen, P.J. Vauhkonen, E. Somersalo and J.P. Kaipio, "Fluid dynamical models and state estimation in process tomography: Effect due to inaccuracies in flow fields", *Department of applied physics report series ISSN 0788-4672*, University of Kuopio, Mar. 2001.

[8] A. Seppänen, M. Vauhkonen, P.J. Vauhkonen, E. Somersalo and J.P. Kaipio, "State estimation with fluid dynamical evolution models in process tomography - EIT application", *Department of applied physics report series ISSN 0788-4672*, University of Kuopio, Jul. 2000.

[9] A. Seppänen, M. Vauhkonen, E. Somersalo and J.P. Kaipio, "State space models in process tomography - approximation of state noise covariance", *Department of applied physics report series ISSN 0788-4672, University of Kuopio*, Oct. 2000.

[10] A. Seppänen, M. Vauhkonen, E. Somersalo and J.P. Kaipio, “State estimation with fluid dynamical evolution models in process tomography – An application with impedance tomography” *Inverse Problems*, vol. 17, pp. 467–483, 2001.

[11] “Nonlinearity-Compensation Extended Kalman Filter and Its Application to Target Motion Analysis”, Oki Electric Industry Co. Ltd., No. 159, Vol. 63, Jul 1997.

[12] M. Vauhkonen, “Electrical impedance tomography and prior information, Ph.D thesis, Kuopio University, Kuopio, 1997.